Effect of temperature on foam flow in porous media

Kapetas, Leon; Vincent-Bonnieu, Sebastien; Danelis, S; Rossen, Bill; Farajzadeh, Rouhi; Eftekhari, Ehsan; Mohd Shafian, SR; Kamarul Bahrim, RZ

Citation (APA)
Kapetas, L., Vincent-Bonnieu, S., Danelis, S., Rossen, B., Farajzadeh, R., Eftekhari, E., Mohd Shafian, SR., & Kamarul Bahrim, RZ. (2016). Effect of temperature on foam flow in porous media. *Journal of Industrial and Engineering Chemistry*, *36*, 229-237. https://doi.org/10.1016/j.jiec.2016.02.001

Important note
To cite this publication, please use the final published version (if applicable).
Please check the document version above.

Effect of temperature on foam flow in porous media

Authors: L. Kapetas[1], S. Vincent Bonnieu[2], S. Danelis[1], W.R. Rossen[1], R. Farajzadeh[1,2], A.A. Eftekhari[1], S. R. Mohd Shafian[3], R. Z. Kamarul Bahrim[3]

1. Department of Geoscience and Engineering, Delft University of Technology, 2.Shell Global Solutions International BV, 3. PETRONAS Research Sdn Bhd

Abstract

Foam can increase sweep efficiency within a porous medium, which is useful for oil-recovery processes[1]. The flow of foam in porous media is a complex process that depends on properties like permeability, porosity and surface chemistry, but also temperature. Although the surface activity of surfactants as a function of temperature is well described at the liquid/liquid or liquid/ gas interface, data on the effect of temperature on foam stability is limited, especially in porous media.

In this work, we tested a surfactant (AOS) at different temperatures, from 20°C to 80°C, in a sandstone porous medium with co-injection of foam. The pressure gradient, or equivalently the apparent viscosity, was measured in steady-state experiments. The core-flood experiments showed that the apparent viscosity of the foam decreased by 50% when the temperature increased to 80°C. This effect correlates with the lower surface tension at higher temperatures. These results are compared to bulk foam experiments, which show that at elevated temperatures foam decays and coalesces faster. This effect, however, can be attributed to the faster drainage at high temperature, as a response to the reduction in liquid viscosity, and greater film permeability leading to faster coarsening.

Our results using the STARS foam model show that one cannot fit foam-model parameters to data at one temperature and apply the model at other temperatures, even if one accounts for the change in fluid properties (surface tension and liquid viscosity) with temperature. Experiments show an increase in gas mobility in the low-quality foam regime with increasing temperature that is inversely proportional to the decrease in gas-water surface tension. In the high-quality regime, results suggest that the water saturation at which foam collapses *fmdry* increases and P_c^* decreases with increasing temperature.

Introduction

Foam is a dispersion of gas bubbles in a continuous liquid medium where bubbles are separated by thin films called lamellae. Foam for Enhanced Oil Recovery (EOR) aims at controlling gas mobility and dealing with phenomena such as gas gravity override, viscous fingering and preferential channeling due to reservoir heterogeneity [2–4]. Despite the fact that active research on foam for EOR has been on the rise, relatively few field or pilot applications have been developed. In the field, foam can be injected by co-injection of gas and surfactant or by surfactant-alternating-gas (SAG) injection. SAG injection with large slugs of liquid and gas injected at the maximum allowable pressure is the preferred approach for field injection to minimize gravity override and time of injection [5].

Bulk foam experiments present foam which is not in contact with the rock, and generally in a tube. Although there is no consensus on the link between bulk and core-floods tests, bulk foam experiments can serve to evaluate foam stability with respect to oil and surfactant type and concentration [6,7], gas composition [8] or temperature. Maini et al. [9] showed that the half-life for foam volume decay in a tube declined dramatically with increasing temperature; sulfonates were found to be clearly superior, and in particular the relative performance of long-chain alpha olefin sulfonates improved with increasing temperature. In their study, Sharma et al. [10] found that the surface tension and bubble size decreased as the temperature increased. With increasing temperature, initial foam volume increased whereas foam half-life (or foam stability) decreased; the difference was more pronounced in the range 20 to 40°C than between 40 and 80°C. The foam film permeability, which is a measure of foam stability, increases with increasing temperature [11]. Foam behavior within a porous medium at reservoir conditions can significantly vary from the bulk experiments, particularly under different thermodynamic conditions [12].

Laboratory core-floods represent a more realistic prediction tool for foam EOR and can serve to quantify foam-model parameters [13]. SAG core-floods can be difficult to interpret because of uncertainties they can introduce: slow foam dynamics in the laboratory due to slow foam generation can introduce significant bias in the results, since local-equilibrium conditions do not apply [14]. Moreover, averaging pressure gradients (or, equivalently, apparent viscosity) throughout the entire core length can introduce bias as separate segments of the core exist at different states; an entrance region can exist where foam never reaches its full strength, and also a capillary end effect can be present at the core outlet controlling liquid saturation which, in turn, influences foam behavior [15].

Steady state co-injection core-floods can be divided in two main categories: (a) constant velocity foam scans, which obtain data at a fixed total superficial velocity while varying gas and liquid superficial velocities [16,17], and (b) experiments which scan the whole liquid velocity vs. gas velocity map. In the latter case the aim is to identify two regimes. In the so-

called "low quality" regime the pressure drop is independent of liquid velocity, and in the "high quality" regime the pressure drop is independent of gas velocity. These experiments are time-consuming and relatively few in the literature; examples of the two regimes are found in the studies [18,19]. The two regimes are reflected also in the constant-velocity foam scans (option (a) above), which was the experimental method chosen for this study.

In modeling foam, Implicit Texture (IT) models are used in most commercial simulators, e.g. STARS (2007)[20]. These models represent the effects of bubble size implicitly through parameters that regulate gas mobility as a function of phase saturations pressure gradient and other factors. These models assume that local steady state is attained instantaneously everywhere in the porous medium. For the purpose of this work only IT models are described and used. They model the effect of foam on mobility by applying a mobility reduction factor (MRF) to the gas relative permeability (or equivalently by increasing gas apparent viscosity). The MRF is a product of different factors/functions which account for the effect of different processes that affect foam behavior, e.g. the presence of oil, surfactant concentration, water saturation or non-Newtonian shear effects (see Appendix A). These functions include a number of parameters. The modeling methods of Boeije and Rossen [21] and Ma et al. [16] have been developed to derive values for some of such parameters by fitting models to the constant velocity foam scan experimental datasets.

This paper investigates the effect of temperature on foam in oil-free core-floods, as well as on bulk foam. The testing hypothesis is that as temperature changes, several effects can take place concurrently which can influence foam performance: modification of interfacial rheology, gas-liquid surface tension, and changes in liquid viscosity are expected to influence foam behavior. For the systems studied, we correlate foam behavior in the core-floods with bulk experimental results.

Methods

The bulk foam experiments were carried out at four different temperatures. The experiment was conducted in a Foamscan apparatus (Teclis instruments), a tube with 3 cm inside diameter with a double wall coupled with a circulating bath controlling the temperature in the column. The surfactant solution was Alpha Olefin Sulfonate (AOS, Bio-Terge 14-16C, Stepan Chemical Co.) 14-16C at 1% active concentration in a 1%w/w NaCl (Merck) solution. The foam was created by sparging gas though a porous glass frit (3 mm thickness with pores size in the range of 100 µm-160 µm)) into 50 ml of surfactant solution which created foam in the tube. During foam generation the gas was injected at a fixed rate of 50 ml/min (standard conditions) and stopped automatically when the foam volume reached 200 ml. Then the liquid fraction in the foam and the foam volume were monitored.

A pair of electrodes at the bottom of the column, immersed in the liquid, measures the drained liquid volume below the foam. The total volume (foam + liquid) was measured with a camera and the volume of the foam at any time was calculated by subtracting the liquid volume from the total volume. Another pair of electrodes were located above the liquid level to measure the liquid fraction in the foam. The electrodes were calibrated with the surfactant solution at the targeted temperature. A temperature sensor inside the tube allowed the measurement of the temperature there.

Surface tension measurements were performed using an EZ-Piplus tensiometer (Kibron Inc.) employing a Du Noüy ring with a microsize probe of 0.51 mm diameter. The instrument was connected to a circulating bath to control the temperature. Once the instrument reached the targeted temperature, the surfactant solution was maintained at that temperature for 30 min before starting the measurements. The surface tension was measured using the Du Noüy method with a microsize probe of 0.51mm diameter.

The core-flood experimental setup is schematically shown in **Figure 1**. Core-flood experiments were carried out using a Bentheimer sandstone core (Kocurek Industries Inc.) of permeability K = 1700 mD, and porosity φ= 0.24. The core was 17 cm long with a diameter of 3.8 cm. The procedure is as follows. A confining pressure is applied to the core for the duration of the experiment. Pressure taps allow pressure-drop measurements in the middle 6.5 cm section of the core. This eliminates entrance-region and capillary end effects. The PEEK core holder is placed in an oven (Memmert) which maintains the temperature constant at the desired value ($\pm 0.1^{\circ}$C). When temperature is changed between experiments a minimum of approximately 1h was allowed to let the core-holder system attain the new temperature. The heat-transfer calculations are decribed in the report of Danelis[13]. A back-pressure regulator controlled the downstream pressure to a nearly constant value of 20±0.3 bar.

The protocol before initiating the foam experiments consisted of the following steps: (i) connection and leakage testing under 20 bar with Helium, (ii) injection of several pore volumes (PV) of CO_2 to displace the air inside the core, (iii) displacement of CO_2 with 6 PV brine at 20 bar back-pressure and (iv) flooding with 5 PV of AOS solution to ensure that adsorption of surfactant on the sandstone was satisfied. Permeability was measured during the last two steps and the foam flooding was then initiated.

Foam quality was controlled by varying the relative rates of injection of N_2 gas and AOS solution, at a constant total superficial velocity. Steady state was considered to be established at a new foam quality when the recorded pressure drop reached a constant value and did not fluctuate (variations less than = ±0.2 bar in a period of 2 h). A mass balance at the effluent location was used to confirm stable saturation once steady state was attained. Pressure drop measurements allow the calculation of the apparent viscosity: this is the value of the pressure gradient normalized with respect to the permeability and the total flux of surfactant solution and gas [16]. Reported apparent viscosity values in this work are calculated based on the pressure drop in the middle section of the core. Gas velocity was calculated from its nominal value by applying two corrections: (i) with respect to the injection pressure set on the Mass Flow Controller, (ii) with respect to the compressibility

factor due to deviation from ideal-gas behavior. The calculation was performed by applying the Jacobsen-Stewart equation of state [22].

Once measurements were completed at a certain temperature, the temperature was raised to the next desired value. A control experiment was carried out with an surfactant solution aged at 80°C. No precipitation was observed and the aged solution was used for a foam scan at 20°C. Aging did not influence the results; hence the surfactant is deemed stable and non-degradable up to 80°C.

Relative permeability for N_2 gas and (surfactant free) brine solution was measured with the unsteady displacement method [23] which allowed the estimation of the Corey parameters, water saturation at residual gas conditions S_{gr}, and connate water saturation, S_{wc}. Values are reported in **Table 1**.
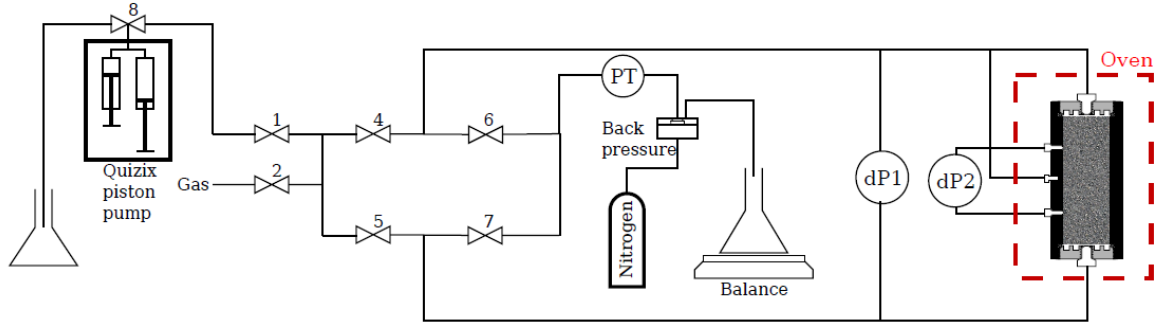
Figure 1. Core-flooding experimental setup: Elements include valves, injection points, core in oven, back-pressure regulator, and effluent collection and weighing.

Parameter	Value
S_{wc}	0.25
S_{gr}	0.20
n_w	2.86
n_g	0.70
k_{rw}^0	0.39
k_{rg}^0	0.59

Table 1. Relative permeability (Corey) parameters.

Mobility reduction factor (MRF) is the reduction in gas mobility caused by foam, relative to gas mobility at the same water saturation in the absence of foam. Foam apparent viscosity is related to MRF by equation 1:

$$\mu_{app}(S_w) = \frac{1}{\dfrac{k_{rw}(S_w)}{\mu_w} + \dfrac{k_{rg}(S_w)}{MRF \times \mu_g}}$$ .... (1)

In the presence of surfactant and absence of oil the STARS foam model [20] in turn relates MRF (its inverse called FM in STARS) to two functions of water saturation and capillary number:

$$MRF = 1 + fmmob \times F_2 \times F_5$$ .... (2)

where *fmmob* is the reference mobility factor, F_2 is a function of water saturation and describes coalescence, and F_5 is a shear-thinning function. Appendix A provides a more detailed description of the model functions F_2 and F_5 and the parameters in those functions. The capillary number, N_{ca}, which represents the balance of viscous forces against surface tension is defined in equation 3:

$$N_{ca} = \frac{\mu_{app} \cdot u}{\sigma_{wg}}$$ .... (3)

where σ_{wg} is the surface tension between the liquid and the gas and u is the total superficial velocity within the porous medium. The calculation of the capillary number at different temperatures serves to normalize the value of the apparent viscosity with respect to surface tension and velocity.

Fitting of the experimental foam scan data was carried out using a constrained non-linear least-squares minimization approach in MATLAB, which simultaneously computes all 5 foam parameters. For this, an initial guess and an allowed range is required for each parameter. Equal weights were assigned to all experimental data during fitting.

Results

Effect of temperature on properties of the surfactant solution. The surface tension and viscosity of the surfactant solution varied remarkably with temperature. As expected [24], the surface tension and viscosity decrease when temperature increases (**Figure 2**). It is noted that the surface tension measurements were not performed at the exact temperature that the core-flood was conducted. Thus, when used later in this section, the surface tension values are interpolated and extrapolated from the curve fitted to data in Figure 2.

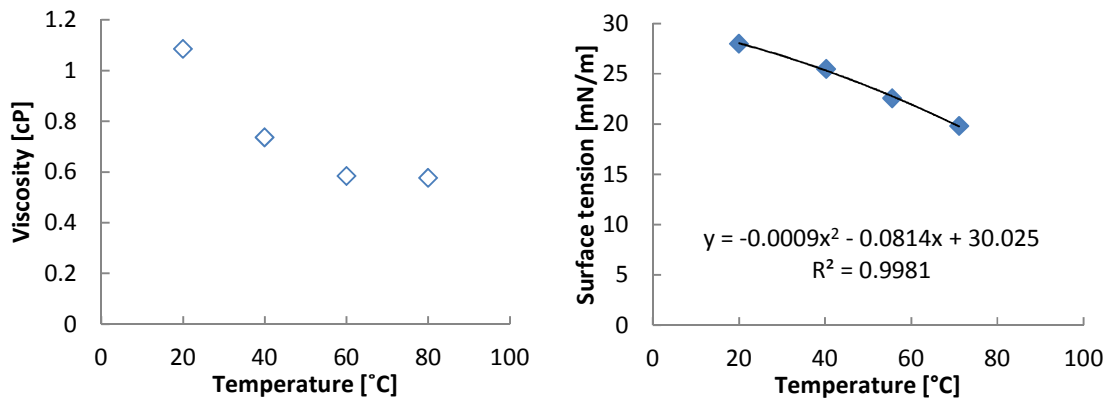$$y = -0.0009x^2 - 0.0814x + 30.025$$
$$R^2 = 0.9981$$

Figure 2. Effect of temperature on the viscosity (left) and the surface tension (right) of the surfactant solution. The size of the markers is larger than the measurement accuracy.

Effect of temperature on bulk foam. The foamability, drainage and stability of the foam were tested using the same surfactant solution and procedure for each temperature.

Foamability. The foamability is the ability to create foam. The foam was created by injecting gas until it reached a volume V_{max} (200 ml) corresponding to a time t_{max}. The foamability is represented by the Foaming Index (FI), where FI is the ratio of foam volume to injected gas volume. The injected gas arrived in the experimental tube at room temperature and was warmed up when it came into contact with the surfactant solution. The injected gas volume was corrected with the ideal gas law, accounting for the temperature difference. With this correction, the FI was not influenced by the temperature (**Figure 3a**).

Foam stability. The foam stability is represented by the foam volume (V) normalized by the maximum volume of the foam column (V_{max}) (**Figure 4**). The foam volume does not depend on temperature at the beginning of the experiments, for times smaller than 200 seconds. After 200 seconds, the foam volume decreases strongly for higher temperatures. The two curves at 53°C are similar at the beginning of the experiment but differ after some time. In one of the two experiments, foam collapses abruptly before the other one. The collapse is due to a cascade of bubbles bursting. In general, the foam volume drops slowly with time at the beginning and dramatically drops at a certain time. The time of the sudden drop fluctuate from one experiment to the other. Despite that foam collapse is not a smooth process, our experiments shows that foam collapse increases with increasing temperature (schematically shown by the arrow in Figure 4). Previous works have shown that the foam stability is influenced by the coupling of coarsening and drainage [25] and also by surface elasticity [26].

Drainage. The foam becomes dryer faster when drainage rate increases, thus destabilizing the foam more rapidly. The effect of the drainage is illustrated by the normalized foam liquid fraction in **Figure 3b**. It appears that drainage rate hardly depends on temperature at the beginning of the experiments, for times below 200 sec. After 200 seconds, the foam liquid fraction dries out faster with increasing temperature, indicating that the drainage rate increases with temperature. The liquid fraction ε is a power law function of time: $\varepsilon \sim t^{\beta}$ [27]. The exponent β usually has a value around (-3) to (-1). t^{β} with an exponent $\beta = -2$ is represented in Figure 3b for comparison with the experiments. Previous work showed that the drainage rate increases with decreasing viscosity of the liquid [27]. In our work, Figure 2a shows that the viscosity of the surfactant decreases with increasing temperature. The increase of the drainage rate can be explained by the decrease of viscosity of the surfactant solution.

Coarsening. Coarsening is due to the pressure differences between the bubbles which results in increasing the average bubbles size. Coarsening increases the drainage rate [27]. The coarsening can be quantified by the critical coarsening time $t_c = L_0^2/[2D_{eff}f(\varepsilon_0)]$ where D_{eff} is the effective film permeability (in our case is $1.67.10^{-5}$), L_0 is the bubble edge length (0.02cm in our experiments) and $f(\varepsilon_0) = (1 - 1.52\varepsilon_0^{0.5})^2$ is the function of the liquid fraction ε_0 (typically 20%) which is discussed in detail in

[28]. The critical coarsening time, t_c, quantifies the importance of coarsening by representing the time above which the coarsening effect is significant. The calculated value of t_c in our experiment is 118 sec. This value of t_c suggests that coarsening is limited during the foaming time because t_c is of the same order as the foaming time, about 200 seconds. Thus, the effect of the coarsening is expected to be significant after 200 seconds. This is observed in Figures 3b and 4, where the effect of temperature is significant after 200 seconds. Furthermore, coarsening is expected to be accelerated at higher temperatures because the foam films' permeability to gas, measured by the film permeability constant, increases with increasing temperature [11]. In others words, temperature increases the films permeability which in turn increases the coarsening of the foam.

To summarize, the bulk foam tests show that the temperature rise increases the drainage rate and destabilizes the foam. These effects can be explained as the effects of temperature on the surfactant viscosity and foam coarsening. The temperature effect on the surface rheology has not been investigated.

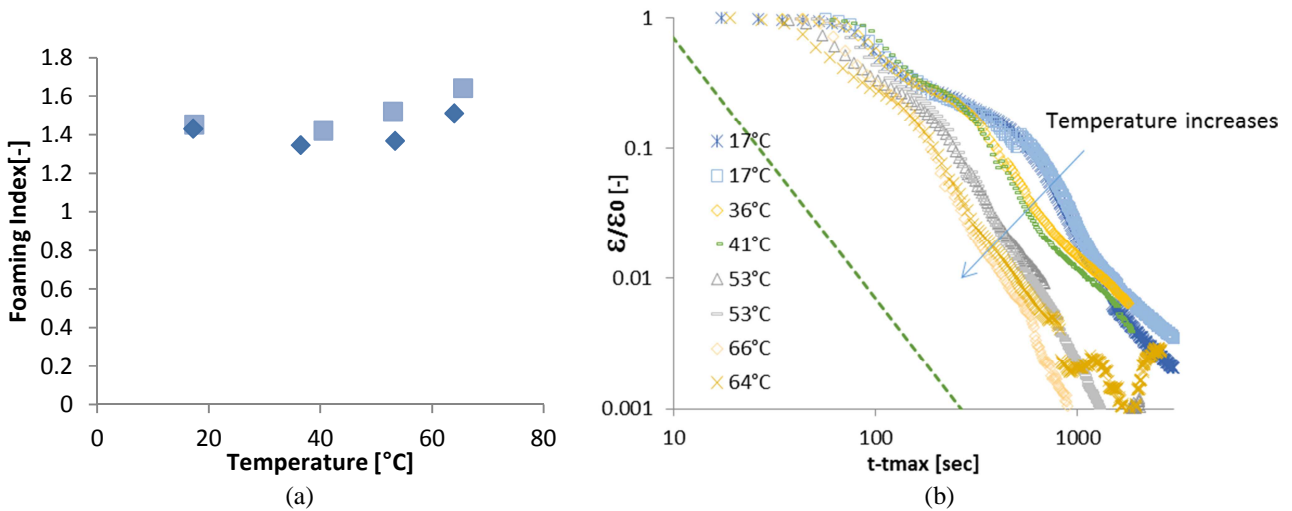(a)   (b)

Figure 3. (a) Foaming Index FI as a function of temperature; each point represents one experiment. (b) Liquid fraction in foam as a function of time for different temperatures. The dashed line represents a power law of time, t^{-2}, for comparison.
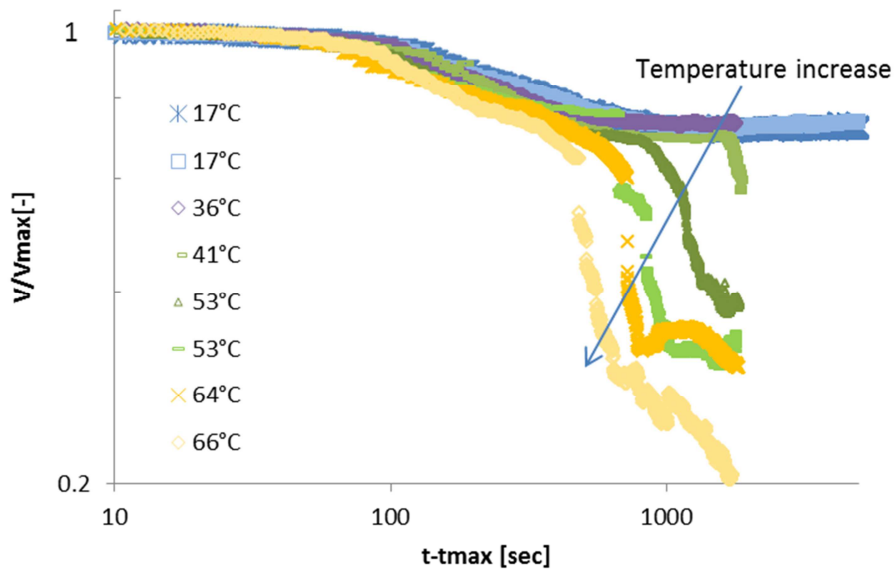

Figure 4. Normalized foam volume as a function of time for different temperatures. Each series represents an experiment.

Effect of temperature on foam in porous media.
Figure 5 shows results for a scan of foam apparent viscosity at constant nominal superficial velocity at four different temperatures (fitted models are discussed later in this section). The foam strength is represented with the apparent viscosity

(in cP) in order to compare the experiments. For example, pressure drops range from 0.3 to 0.5 MPa for the coreflood of Bentheimer rock at 20°C. In general the viscosity increase first with foam quality and then decrease sharply. This is because, under steady-state conditions, foam exhibits two flow regimes depending on gas fractional flow (i.e. foam quality) [19]. In the so-called low-quality regime (low gas fraction), the pressure gradient increases as the gas saturation rises because the foam volume increases. As the quality increases, the capillary pressure increases [29]. Foam collapses at the transition between regimes (at the maximum of apparent viscosity occurs because the capillary pressure exceeds the critical capillary pressure Pc*. Transition happens at the critical water saturation Sw* (the water saturation corresponding to Pc*). In the high quality regime (high gas fraction), the capillary pressure exceeds Pc* which destabilize the foam, decreasing the apparent viscosity. For the low-quality regime (portion of data to left of maximum), it is noted that as temperature increases from 20 to 80°C the measured apparent viscosity of the foam decreases. The size of the decrease, between the experiments carried out at 20 and 80°C, is of the order of 50%. It is possible that the lowering of the surface tension (Figure 2b, **Table 2**) allows a less-restricted flow of the foam.
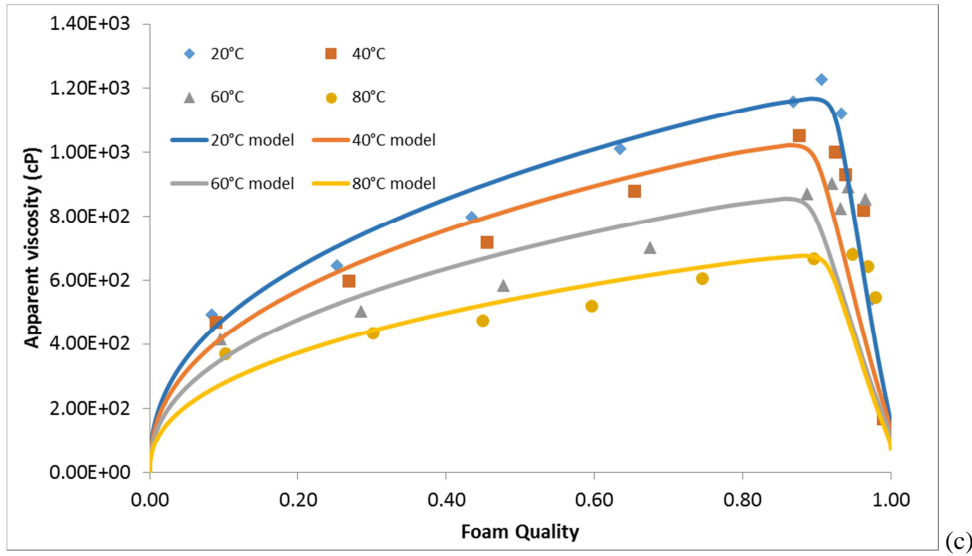

(a)

(b)

(c)
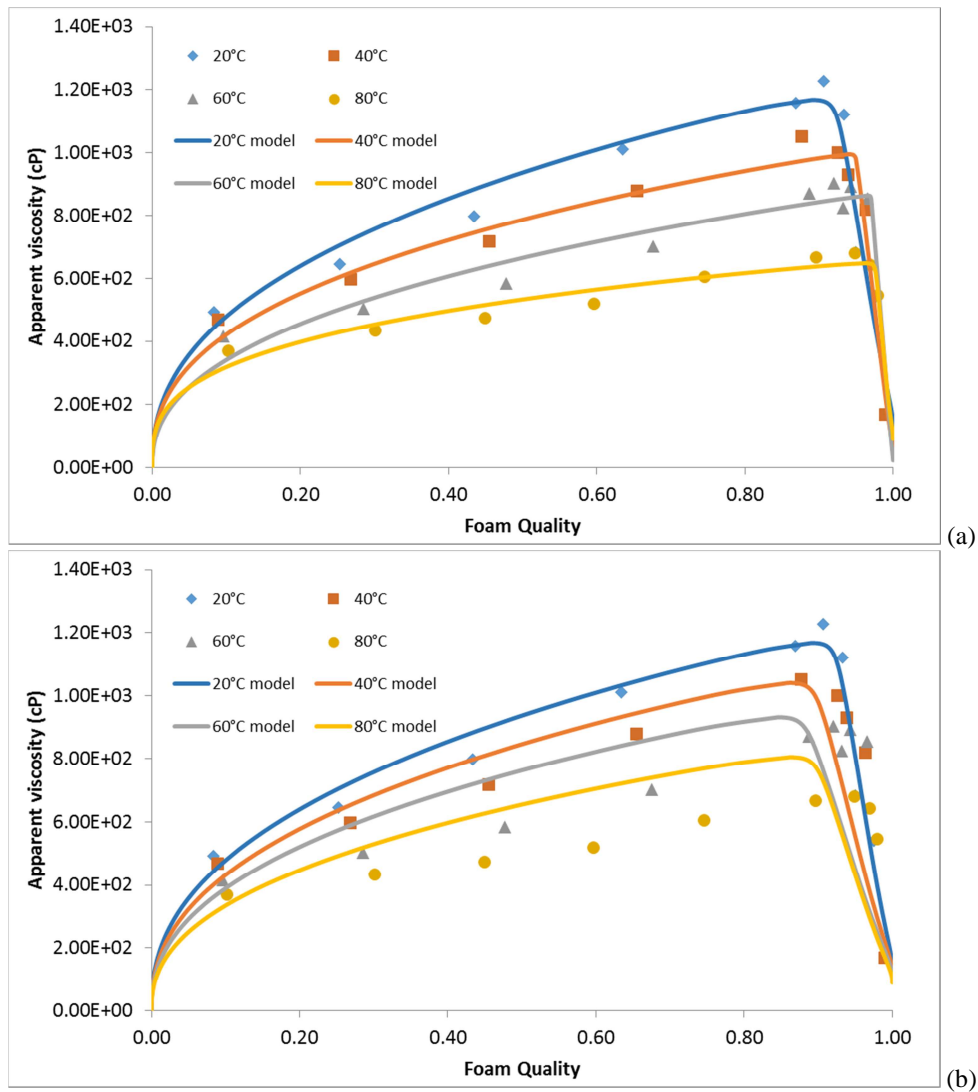
Figure 5. Measured apparent viscosity against foam quality for constant-velocity foam scans at different temperatures (data-points). Lines represent models fitted using the least-squares minimization method (a) by adjusting all foam parameters, (b) by keeping their values constant and equal to their optimized value for the experiment at 20°C, among all temperatures and (c) by treating only *fmcap* as an adjustable parameter; all other foam parameters were kept constant and equal to their optimized value for the experiment at 20°C (see text for the model parameterization approach).

Parm/T	20 °C	40 °C	60 °C	80 °C
u (ft/day)	3.92E+00	4.16E+00	4.29E+00	4.58E+00
μ_w *(mPa·s)*	1.08E+00	7.30E-01	5.80E-01	5.70E-01
σ *(mNt/m)*	2.80E+01	2.53E+01	2.19E+01	1.78E+01

Table 2. Mean velocity values at the middle section of the core (for all the different foam qualities, see Figure 6), surface tension and liquid viscosity for each temperature used as measured input parameters to the STARS foam model using the least-squares minimization method.

The transition foam quality (i.e., quality at the peak in apparent viscosity), f_g^*, is approximately the same for all temperatures, i.e. 0.93±0.03. The decreasing slope of the curves as foam quality increases towards f_g^* reflects shear thinning behavior of foam in the low-quality regime. Increasing pressure gradient allows gas to flow more easily in pores already opened to flow [30] and in additional pores opened to flow by the higher pressure gradient [31]. Thus apparent mobility is shear-thinning with respect to gas flow rate both due to increasing pore pathways available for flow as pressure gradient increases and the shear-thinning rheology along each pathway [32].

Gas compressibility caused actual gas superficial velocity to deviate from intended values, especially at the largest pressure drops (largest apparent viscosities), as shown in **Figure 6**. The largest pressure drops along the core in our experiments as about 1.3 MPa , though the pressure rise in the ceral section in which pressure-differences were measured was less. The deviations were less at higher temperatures. Mean velocity values for the middle section of the core for each temperature are reported in Table 2, with a maximum difference of 17% between experiments at 20 and 80°C. Viscosity values reported (Figure 5) where computed based on the velocity (accounting for gas compression) obtained at each individual foam quality and temperature. For a shear-thinning foam, a velocity decrease can lead to an increase in viscosity. Thus, since a shear-thinning behavior is observed in our experiments we expect that it partially contributes to the reduction of apparent viscosity in the higher-temperature experiments.

Increasing temperature induced a reduction in surface tension, which in turn affects the capillary number, N_{ca}, of the displacement; **Figure 7a** presents the experimental results of Figure 5 in terms of N_{ca}. Notably, the product of apparent viscosity and N_{ca} collapses onto a single curve, which suggests that apparent viscosity is proportional to surface tension in our experiments, once results are normalized for velocity (as by definition done in the capillary number calculation). The effect of the surface tension on the apparent viscosity could be explained by the variation of film elasticity which is related to surface tension as proposed in previous works [7,33]. The apparent viscosity observed in the coreflood could also be related to the force required to stretch the foam film (called surface elasticity). The apparent viscosity in the coreflood would increase as the elasticity increases. In our experiment, the elasticity was not measured but we could speculate the elasticity varies like surface tension [4]. **Figure 7b** presents this relationship between apparent viscosity and measured surface tension (at the experimental temperature values) for a 60% foam quality: the monotonic relationship is clear.
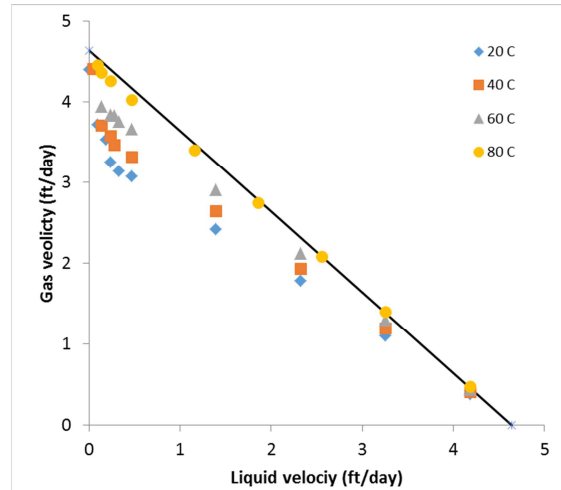
Figure 6. Liquid vs. gas velocity for the experimental data of Figure 5 obtained at different temperatures. Straight line represents a constant total flow rate of 4.64 ft/day. Actual superficial velocities deviate somewhat from the nominal values.
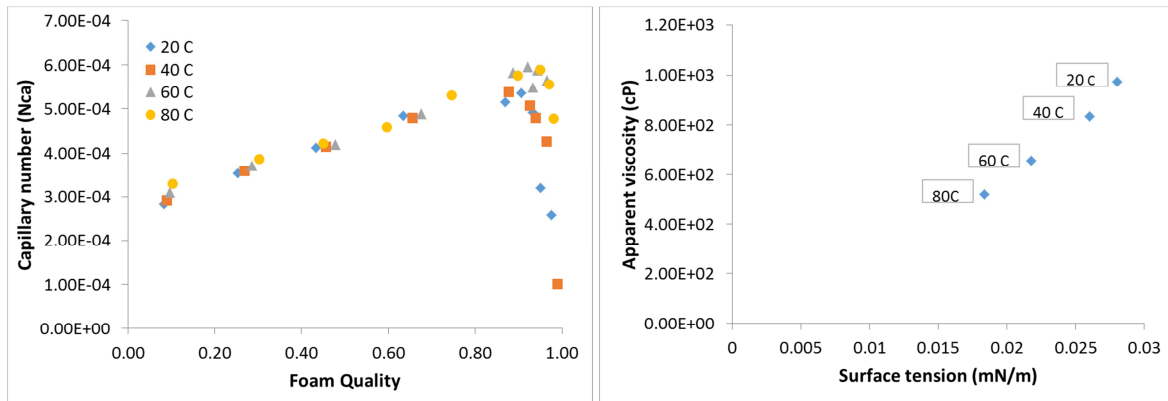

Figure 7. (a) Capillary number vs. foam quality at different temperatures; data are from Figure 5. (b) Apparent viscosity at fixed foam quality, f_g = 0.60, vs. surface tension as affected by changes in temperature.

Modelling. The foam-model equations, as presented in Section 2 and Appendix A, are used to provide an interpretation of the effect of temperature on foam mobility. More specifically, we aim to establish the effect of temperature on foam-model parameters. Three different approaches were followed to fit the experimental data:

(1)   All foam-model parameters were treated as adjustable. Their optimal values are shown in Table 3 and plotted in the figure 8. The results obtained were robust: the initial guess and range values provided did not influence the parameter values, suggesting a global optimum solution. The liquid viscosity and the surface tension were adjusted to their experimentally measured values (Table 2). The former is used in the calculation of the water relative permeability and the latter is used in the calculation of N_{ca} within function F_5. Figure 5a presents the model fits. The models provide a good fit to all datasets under this fitting approach. The change of apparent viscosity in the high-quality regime (to the right of the maximum) can be effectively represented by a single straight line through ($f_g = 1$, $\mu_{app} = 0$) for all temperatures (cf. [21]). The trend of fitted parameters with temperature is shown in Figure 8. Parameter *fmdry* (the water saturation around which foam collapses) decreases slightly (from 0.277 to 0.267), but these values are close to irreducible water saturation (Table 1); therefore this decrease is enough to make a difference of almost a factor of 4 in water relative permeability in the high-quality regime.

        The modeling results of Figure 5a are in close agreement with the results obtained using the method of Boeije and Rossen [21] (see Appendix B). Their method requires a large value of *epdry*. The least-squares minimization method used here is able to fit data with smaller values of *epdry*, allowing a smoother transition between the low- and high-quality regimes. Like the method of Boeije and Rossen, the method can accommodate shear-thinning behavior in the high-quality regime.

(2)   To investigate the ability of the model to predict the effect of surface tension alone on the apparent viscosity, a second fitting exercise was conducted as follows. All foam model parameters were kept constant between experiments at different temperatures, equal to the values obtained by fitting the model to the 20°C data in Table 3. Surface tension and liquid viscosity were adjusted for the effect of temperature using Figure 2. Figure 5b shows that the models at 40, 60 and 80°C do not provide good fits. In the low-quality regime, apparent viscosity is overestimated. Moreover, in the high-quality regime, the model deviates from the data; holding *fmdry* fixed does not account for the nearly fourfold change in k_{rw} in this

regime as temperature increases. One cannot fit these foam model parameters at one temperature and apply them with confidence to other temperatures, even if one accounts for the effect of temperature on surface tension and liquid viscosity.

(3)   A third modeling approach investigates the effect of temperature on specific parameters. In this case, for the model fitting of the experimental data at 40, 60, 80 $^{\circ}$C, values for all the parameters were kept constant and equal to the optimized parameters obtained at 20°C (Table 3), except for *fmcap* (the only fitted parameter). This is equivalent to adjusting *fmmob*, since only the product of these two parameters *fmmob*×F_5 matters in Eq. A1. The model fits are shown in Figure 5c. The rationale for treating *fmcap* as an adjustable parameter is to identify if a direct correlation between temperature and a foam parameter exists. In this case *fmcap* is predicted to decrease with increasing temperature with values of 2.53x10^{-4}, 2.44x10^{-4}, 2.15x10^{-4}, and 1.82x10^{-4} for the 20, 40, 60, 80°C experiments respectively. The model fits are as good as in Figure 5a in the low-quality regime. Because of the equivalence of adjusting *fmcap* and *fmmob* in this model, in effect, these results suggest that *fmmob* is inversely proportional to gas-water surface tension. In the high-quality regime, they deviate from the data because they do not account for the decrease in *fmdry* and water relative permeability.

In the STARS foam model, parameter *fmdry* is related to the collapse of foam at the limiting capillary pressure P_c^* [29,34]. In the limit of large *epdry*, *fmdry* is the water saturation at P_c^*. In our model fits, *fmdry* decreases slightly with increasing temperature, but its value is close to irreducible water saturation. A constant value of *fmdry*, together with the decrease in surface tension (Figure 2) would imply a reduction in P_c^* by about a 25% from 20°C to 80°C; in other words, foam is less stable at higher temperature. However, we don't know how sensitive capillary pressure is to water saturation so close to irreducible water saturation, so the trend of P_c^* with temperature cannot be determined from these data with confidence. One can conclude that *fmdry*, the parameter needed to represent foam flow directly, does decrease with increasing temperature in these data; the poor fit to the high-quality regimes in Figures 2b and 2c make this clear.

Parm/T	20°C	40°C	60 $^{\circ}$C	80°C
fmmob	1.14E+05	2.01E+05	1.04E+05	1.70E+05
epdry	2.36E+03	2.42E+04	9.78E+04	7.43E+03
fmdry	2.77E-01	2.71E-01	2.67E-01	2.68E-01
fmcap	2.53E-04	1.65E-04	2.12E-04	2.05E-04
epcap	1.33E+00	1.51E+00	1.34E+00	2.04E+00

Table 3. Optimal values for all foam parameters as calculated by fitting the experimental data with the least-squares minimization method. Model fits presented in Figure 5a.
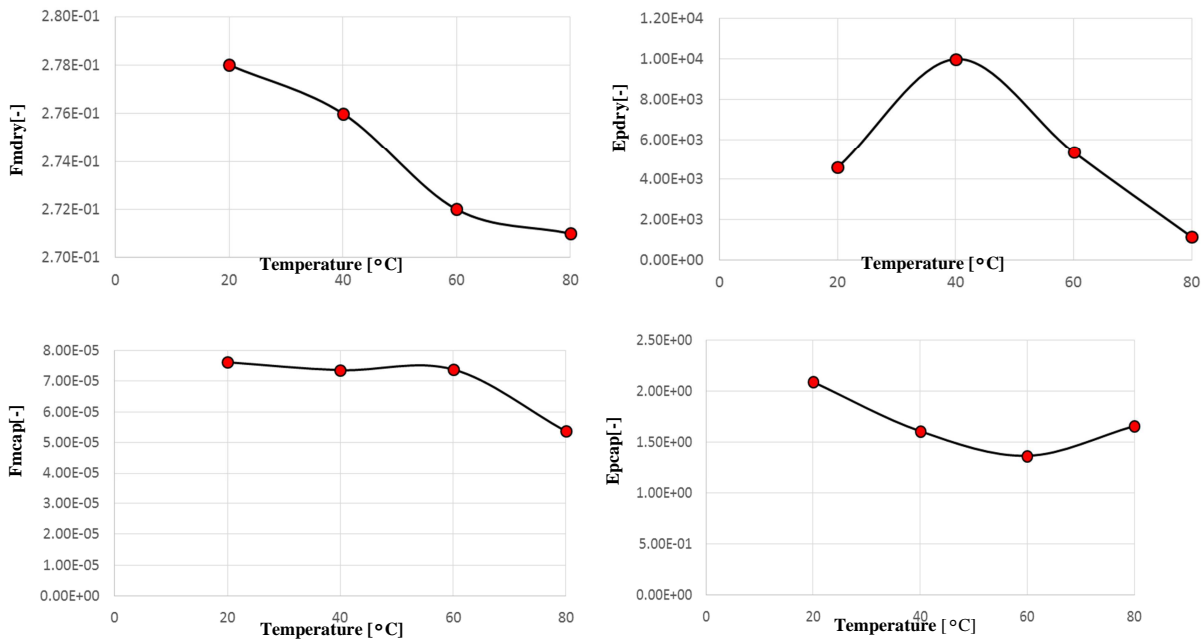
Figure 8. Changes in the five foam parameters with respect to temperature changes for Bentheimer sandstone

Conclusions and Implications

This study presents a combination of bulk and core-flood experimental methods to investigate the effect of temperature on the foaming ability and mobility of foam for a specific surfactant. The bulk foam experiments show that foam decays faster and drainage increases as temperature increases. This can be attributed to reduced liquid viscosity leading to faster drainage rates of the surfactant solution and the increased film permeability leading to an increase of coarsening. The relation between drainage from bulk foam, over a distance of cm, driven by gravity, to drainage from foam films in porous media, over a distance of 100's μm, driven by capillary pressure, is not simple, however.

The results in this work indicate that it is critical that laboratory core-floods be at conditions which approximate the physical conditions of the reservoir under study. Specifically, the behavior of foam was shown to be influenced by temperature changes. In our study the change in foam behavior with temperature could not be predicted simply from changes in liquid viscosity and surface tension, holding other foam parameters constant. Although large temperature differences are not expected within a single reservoir, caution should be taken in extrapolating foam parameters to temperatures different from those studied in the laboratory. Understanding the effect of temperature on foam and incorporating this effect mechanistically in reservoir simulations will require further experimental research.

Acknowledgements

Nomenclature

SI units are assumed for all parameters used in calculations.

$epcap$	Foam parameter controlling shear thinning
$epdry$	Foam parameter controlling abruptness of foam collapse
$fmcap$	Foam parameter assumed equal to smallest expected capillary number
$fmmob$	Reference mobility reduction factor
$fmdry$	Critical water saturation at which foam collapses
FI	Foaming Index
MRF	Mobility Reduction Factor
k_{rg}	Relative permeability of gaseous phase in absence of foam
k_{rg}^0	End-point relative permeability of gaseous phase
k_{rw}	Relative permeability of aqueous phase
k_{rw}^0	End-point relative permeability of aqueous phase
N_{ca}	Capillary number
n_g	Exponent in k_{rg} curve
n_w	Exponent in k_{rw} curve
S_{gr}	Residual gas saturation
S_w	Water saturation
S_{wc}	Connate water saturation
t	Time (s)
u	Darcy velocity (ft/day)
V	Volume (mL)
ε	Liquid fraction
φ	Porosity
μ_g	Viscosity of gas (cP)
μ_w	Viscosity of water (cP)
μ_{app}	Average apparent foam viscosity for middle core section (cP)
σ_{wg}	Surface tension (mN/m)

References

[1] R. Farajzadeh, A. Andrianov, R. Krastev, G.J. Hirasaki, W.R. Rossen, Adv. Colloid Interface Sci. 183–184 (2012) 1–13. 10.1016/j.cis.2012.07.002.

[2] W.R. Rossen, Foams: Theory: Measurements: Applications, Marcel Dekker, Inc., New York - Basel, 1995, .

[3] Laurier L. Schramm, Fred Wassmuth, Foams: Fundamentals and Applications in the Petroleum Industry, Vol. 242, American Chemical Society, 1994, pp. 3–45.

[4] L.L. Schramm, Surfactants Fundamentals and Applications in the Petroleum Industry, Cambridge University Press, Calgary, Canada, 2000.

[5] D. Shan, W.R. Rossen, SPE J. 9(02) (2004) 132–50. 10.2118/88811-PA.

[6] A.K. Vikingstad, A. Skauge, H. Høiland, M. Aarra, Colloids Surf. Physicochem. Eng. Asp. 260(1-3) (2005) 189–98. 10.1016/j.colsurfa.2005.02.034.

[7] S.A. Jones, G. Laskaris, S. Vincent Bonnieu, R. Farajzadeh, W.R. Rossen, Vol. SPE-179637-MS, Society of Petroleum Engineers, Tulsa, USA, 2016, .

[8] R. Farajzadeh, S. Vincent-Bonnieu, N. Bourada Bourada, J. Soft Matter 2014 (2014) e145352. 10.1155/2014/145352.

[9] B.B. Maini, V. Ma, J. Can. Pet. Technol. 25(06) (1986). 10.2118/86-06-05.

[10] M.K. Sharma, D.O. Shah, W.E. Brigham, AIChE J. 31(2) (1985) 222–8. 10.1002/aic.690310208.

[11] R. Farajzadeh, R. Krastev, P.L.J. Zitha, Langmuir 25(5) (2009) 2881–6. 10.1021/la803599z.

[12] M. Chabert, L. Nabzar, V. Beunat, E. Lacombe, A. Cuenca, Society of Petroleum Engineers, 2014, .

[13] S. Danelis, L. Kapetas, S. Vincent-Bonnieu, W.R. Rossen, Temperature effect on foam coreflood experiments, TU Delft, Civil Engineering and Geosciences, Geotechnology, 2015.

[14] L. Kapetas, W.A. van El, W.R. Rossen, Society of Petroleum Engineers, 2014, .

[15] O.G. Apaydin, A.R. Kovscek, Transp. Porous Media 43(3) (2001) 511–36. 10.1023/A:1010740811277.

[16] K. Ma, J.L. Lopez-Salinas, M.C. Puerto, C.A. Miller, S.L. Biswal, G.J. Hirasaki, Energy Fuels 27(5) (2013) 2363–75. 10.1021/ef302036s.

[17] A. Moradi-Araghi, E.L. Johnston, D.R. Zornes, K.J. Harpole, Society of Petroleum Engineers, 1997, .

[18] W.T. Osterloh, M.J. Jante Jr, others, SPE/DOE Enhanced Oil Recovery Symposium, Society of Petroleum Engineers, 1992, .

[19] J.M. Alvarez, H.J. Rivas, W.R. Rossen, others, SPE J. 6(03) (2001) 325–33.

[20] Computer Modelling Group Ltd., User's Guide STARS, Calgari, Canada, 2009.

[21] C.S. Boeije, W. Rossen, SPE Reserv. Eval. Eng. 18(02) (2015) 264–72. 10.2118/174544-PA.

[22] R.T. Jacobsen, R.B. Stewart, J. Phys. Chem. Ref. Data 2(4) (1973) 757–922. 10.1063/1.3253132.

[23] E.F. Johnson, D.P. Bossler, V.O.N. Bossler, (1959).

[24] J.J. Bikerman, Surface Chemistry (Second Edition), Academic Press, 1958, pp. 1–135.

[25] A. Saint-Jalmes, Soft Matter 2(10) (2006) 836. 10.1039/b606780h.

[26] D. Georgieva, A. Cagna, D. Langevin, Soft Matter 5(10) (2009) 2063–71. 10.1039/B822568K.

[27] A. Saint-Jalmes, D. Langevin, J. Phys. Condens. Matter 14(40) (2002) 9397.

[28] S. Hilgenfeldt, S. Koehler, H. Stone, Phys. Rev. Lett. 86(20) (2001) 4704–7. 10.1103/PhysRevLett.86.4704.

[29] Z.I. Khatib, G.J. Hirasaki, A.H. Falls, others, SPE Reserv. Eng. 3(03) (1988) 919–26.

[30] G.J. Hirasaki, J.B. Lawson, Soc. Pet. Eng. J. 25(02) (1985) 176–90. 10.2118/12129-PA.

[31] G.-Q. Tang, A.R. Kovscek, Transp. Porous Media 65(2) (2006) 287–307. 10.1007/s11242-005-6093-4.

[32] W.R. Rossen, M.W. Wang, SPE J. 4(02) (1999) 92–100. 10.2118/56396-PA.

[33] L.L. Schramm, W.H.F. Green, Colloids Surf. Physicochem. Eng. Asp. 94(1) (1995) 13–28. 10.1016/0927-7757(94)02997-7.

[34] L. Cheng, A.B. Reme, D. Shan, D.A. Coombe, W.R. Rossen, Society of Petroleum Engineers, 2000, .

[35] Z. Zhou, W.R. Rossen, SPE Adv. Technol. Ser. 3(01) (1995) 154–62. 10.2118/24180-PA.

Appendix A.

The Local Equilibrium STARS model used in this study is described by [20,21,34]. The STARS model introduces the MRF function (inverse of mobility factor *FM* in STARS) which describes the reduction in gas mobility by foam (Eq. 1). The full version of the MRF function is given by

$$MRF = 1 + fmmob\ F_1\ F_2\ F_3\ F_4\ F_5\ F_6 \quad\text{.. (A1)}$$

The parameter *fmmob* is the reference gas mobility-reduction factor for wet foams. This parameter corresponds to the maximum attainable mobility reduction. The functions F_1-F_6 are constrained to values less than or equal to 1, so that each function can only reduce the gas mobility-reduction factor, i.e. increase gas mobility. The functions model the effect of surfactant concentration (F_1), effect of water saturation on foam properties (F_2), oil saturation (F_3), gas velocity (F_4), capillary number (F_5) and the critical capillary number (F_6). In the present work F_2 and F_5 are considered and defined with equations A2 and A3 respectively:

$$F_2 = 0.5 + \frac{\arctan\left(epdry\left(S_w - fmdry\right)\right)}{\pi} \quad\text{.. (A2)}$$

$$F_5 = \left(\frac{fmcap}{N_{ca}}\right)^{epcap} \quad\text{.. (A3)}$$

Thus the foam model we use contains five parameters, namely *fmmob, epdry, fmdry, fmcap and epcap*.

- *epdry* controls the abruptness of the foam collapse as a function of water saturation. Small values give a gradual transition between the two regimes, while larger values yield a sharper, albeit still continuous, transition.

- If the transition between regimes is abrupt, the parameter *fmdry* is equal to S_w^*, the water saturation at the limiting capillary pressure P_c^*, i.e. the water saturation at which foam collapses [35].

- *fmcap* represents the lowest capillary number expected in the simulation and below this value shear thinning behavior is not expected. Thus *fmcap* is not considered a foam parameter per se. Parameter *epcap* controls the significance of shear thinning; the larger it is, the stronger the shearing thinning behavior becomes.

Appendix B.

A comparison between the model fitting results of the least-squares minimization method and the method of Boeije and Rossen [21] is provided in more detail in this section. The latter method assumes an abrupt collapse at the critical capillary pressure condition. We model the experimental data with both methods and proceed to a comparison of the parameter values. **Figure B1** shows that the two model fits are in good agreement with each other and with the experimental data set. The same conclusion is reached for the experimental data at the higher temperatures (results not shown). As *fmcap* is not a foam parameter *per se*, its value is fixed between the two methods (equal to its adjusted value from the least-squares minimization method, see **Table B1**). The value of *fmdry* is predicted to be the same by the two methods. The values of *fmmob* and *epcap* are in close agreement, which is also suggested by the model fits; the former mostly controls the magnitude of the model apparent viscosity in the low-quality regime and the latter the shear thinning behavior. *epdry* is not calculated with the model of Boeije and Rossen [21]; rather it is assumed to be large enough to lead to an abrupt foam collapse during regime transition as mentioned above. Its value optimized using the least-squares minimization method suggests the transition is relatively abrupt.
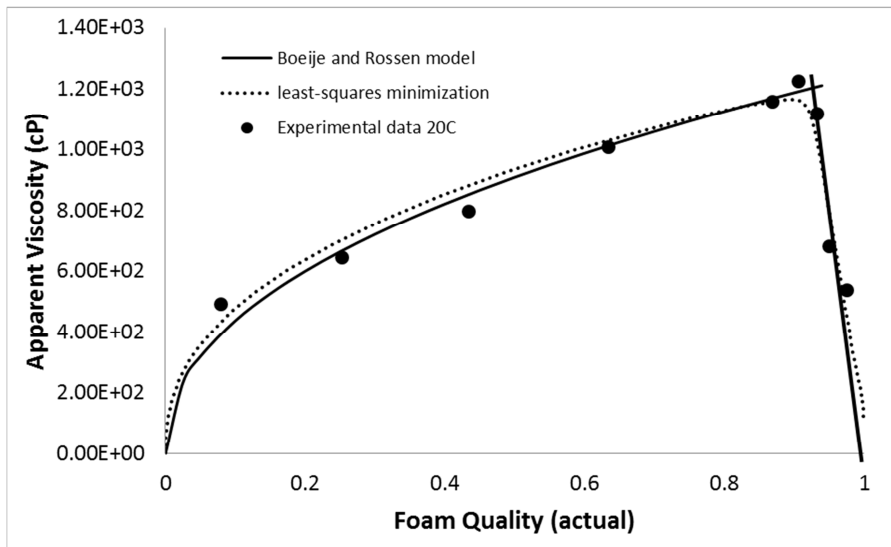
Figure B1. Comparison between the model fits of Boeije and Rossen [21] **and least-squares minimization to the experimental data of the foam scan conducted at 20ºC.**

Parm	Boeije and Rossen	Least-squares
fmmob	1.03E+05	1.14E+05
epdry	high	2.36E+03
fmdry	2.77E-01	2.77E-01
fmcap	2.53E-04	2.53E-04
epcap	1.21E+00	1.33E+00

Table B1. Comparison between optimized foam parameters obtained with the methods of Boeije and Rossen [21] **and least-squares minimization, fitted to the data of Figure B1.**